Impact of the non-axisymmetric SOL current driven by a biased electrode on the diverted J-TEXT plasma

Shuhao Li[1], Nengchao Wang[1,*], Yonghua Ding[1,*], Yunfeng Liang[1,2,3], Qinghu Yang[1], Feiyue Mao[1], Xin Xu[1], Zhengkang Ren[1], Chuanxu Zhao[1], Zhuo Huang[4], Abba Alhaji Bala[1,5], Zhipeng Chen[1], Zhongyong Chen[1], Zhoujun Yang[1], Yuan Pan[1] and the J-TEXT team[†]

[1] International Joint Research Laboratory of Magnetic Confinement Fusion and Plasma Physics, State Key Laboratory of Advanced Electromagnetic Engineering and Technology, School of Electrical and Electronic Engineering, Huazhong University of Science and Technology, Wuhan, 430074, People's Republic of China

[2] Institute of Plasma Physics, Chinese Academy of Sciences, Hefei 230031, People's Republic of China

[3] Forschungszentrum Jülich GmbH, Institut für Energie- und Klimaforschung - Plasmaphysik, 52425 Jülich, Germany

[4] College of Computer Science, South-Central Minzu University, Wuhan, 430074, People's Republic of China

[5] Physics Department, Federal University Dutse, Dutse, Jigawa, Nigeria

E-mail: wangnc@hust.edu.cn and yhding@hust.edu.cn

Abstract

To study the effect of the scrape-off layer (SOL) current on the plasma boundary and strike points, two rounds of SOL biasing experiments are conducted on the J-TEXT tokamak. In the experiments, the plasma parameters of SOL and the strike points on the target plate are significantly changed, which is caused by the magnetic and electrostatic effects caused by the SOL current driven by the biased electrode (EB). During the application of positive bias to the biased electrode, the CCD camera captured the upper strike points splitting on the divertor target plate, which generally occurs in the resonant magnetic perturbations (RMPs) experiment. In addition, the SOL plasma parameters measured by the reciprocating probe, such as floating potential (V_f), electron temperature (T_e), and ion saturation current (I_s), are significantly altered by applying modulation bias, which is closely related to the SOL current. A SOL current model has been developed in the limiter configuration on J-TEXT. Now this model is extended to the poloidal divertor configuration to meet the experimental simulation requirements, which can calculate the magnetic field generated by SOL current and the change of magnetic topological structure of plasma boundary. The simulation results show that the magnetic perturbation

* Authors to whom any correspondence should be addressed.

† See the author list of "Y. Liang *et al* 2019 Overview of the Recent Experimental Research on the J-TEXT Tokamak, *Nucl. Fusion* 59 112016"

generated by the SOL current causes the formation of lobes near the X-point, which is three-dimensional asymmetric structure. Since there is no edge-localized modes (ELMs) on the J-TXET tokamak, the change in the boundary magnetic topology potentially demonstrates that the SOL current is capable of generating sufficiently strong magnetic perturbations can be used as another alternative method to control the ELMs.

1. Introduction

In future fusion reactors like ITER, edge-localized modes (ELMs) is an inevitable boundary magnetohydrodynamics (MHD) instability [1]. It will bring transient thermal load to the plasma-facing components (PFC) and divertor target plate, which will exceed the tolerance limit of the target plate material and threaten the steady-state operation of the reactors. Experiments using resonant magnetic perturbations (RMPs) or lower hybrid wave (LHW) to control ELMs have been carried out on many devices such as JET [2-3], AUG [4], EAST [5-6], KSTAR [7], DIII-D [8-10], MAST [11]etc. Moreover, it has also been observed that the non-axisymmetric perturbed magnetic field will form lobes near the X-point and lead to the strike points splitting [12-17]. Evans' study shows that non-axisymmetric magnetic perturbations cause overlapping stable and unstable manifolds at the plasma separatrix to cross to form lobes known as homoclinic tangles [18]. It is also observed that the LHW will drive the scrape-off layer (SOL) current with amplitude of 1kA on EAST [19-20], and the SOL current can generate strong magnetic perturbation, forming three-dimensional asymmetric lobes near X-point. Experiments using SOL current driven by biased target plates or biased electrodes (EB) to investigate the effect on boundary plasma or the thermal load of divertor target plates have been carried out in some fusion devices such as NSTX [21-22], JFT-2M [23-24], TORPEX [25-26], MAST [27], COMPASS-D [28-29], DIII-D [30]. More recently, the interaction between SOL current or current driven by biased electrode and MHD mode has also been studied on HBT-EP [31-32]. On the HL-2A tokamak, biased target plates have been installed to study the effect of control on ELMs [33]. In the J-TEXT tokamak [34-35], the electrode biasing auxiliary system has been installed on it [36]. Experiments using biased electrode to control tearing modes (TMs) and improve plasma confinement have also been carried out on J-TEXT [37-39]. In the limiter configuration, it has

been proved that the electrode can drive the non-axisymmetric SOL current on J-TEXT [40-41], and the magnetic perturbation caused by the SOL current is also measured by poloidal magnetic probe array [42]. In this manuscript, we mainly focus on the effect of SOL current driven by the biased electrode on the strike points splitting in poloidal divertor configuration, which indicates that SOL current may be a new method to control the ELMs instead of the traditional magnetic perturbation coil due to its strong boundary resonance component [43-45].

The J-TEXT tokamak mainly conducts discharge experiments in the limiter configuration. In the last two years, physical experiments and simulations in the poloidal divertor configuration started to be carried out [46]. Meanwhile, SOL biasing experiments in the divertor configuration are also carried out. This paper presents the experimental results of the first observation of the SOL current driven by the biased electrode in divertor configuration on J-TEXT. The poloidal divertor configuration and experimental setup are described in section 2. In section 3, the results of experiment and simulation are divided into three parts. Section 3.1 is the basic characteristics of SOL current, section 3.2 is the influence of SOL current on plasma parameters, and section 3.3 shows the changes of SOL currents on the boundary magnetic topology and its induced the strike points splitting. Finally, the experimental results are discussed and summarized in section 4 and section 5 respectively.

2. The experimental set-up on J-TEXT

The J-TEXT tokamak is a conventional iron core tokamak with a major radius $R_0 = 1.05$ m and a minor radius a = 25-29 cm, using removable titanium carbide coated graphite limiters. It also has an electron cyclotron resonance heating (ECRH) auxiliary heating system with a maximum power of 500 kW. Typical plasma parameters of J-TEXT discharge are: The electron temperature of the core plasma is 1 keV, the electron density of the core plasma is $0.5\text{-}7\times10^{19}$ m^{-3}, the electron temperature of SOL plasma is 10-50 eV, and the ion temperature is 20-80 eV. The 16 toroidal field coils can generate the toroidal field of 1.2-2.5 T, and the plasma current generated by the central solenoid is 100-230 kA. As shown in figure 1, J-TEXT is composed of two vacuum chambers, and the joints of the two vacuum chambers are insulated by keystone. Two vacuum chambers with 7 ports each 14 ports in total, 24 silicon carbide graphite target plates connected to

the stainless steel vacuum chamber are installed on the high field side, and three limiters are installed on port 14. The biased electrode made of graphite is installed 80 mm below the middle plane on the low field side of port 8 . The biased electrode power supply is capable of outputting up to 900V and over 200kW of power. Two reciprocating probes are installed on the upper part of port 12 and port 13 respectively, which are mainly used to measure boundary plasma parameters. The CCD camera is mounted on the middle plane of port 12, which is used to photograph the visible light radiation generated by hydrogen plasma in the vacuum chambers, especially the radiation near the strike points or at the plasma boundary. Moreover, the lens of CCD camera can be added H_α or C_{III} filter to observe a certain visible light radiation. Fifteen sets of divertor Langmuir probes (DLP) are mounted only on the high-field side target plate of port 9 to measure divertor plasma parameters. Two poloidal magnetic probe arrays are installed at port 2-3 and port 10-11 respectively, which are mainly used to analyze the magnetohydrodynamics (MHD) instabilities of plasma such as tearing modes (TMs) and alfven eigenmodes (AEs). The black arrow in figure 1 defines the direction of the plasma current and the toroidal field as counterclockwise (+φ) on J-TEXT.

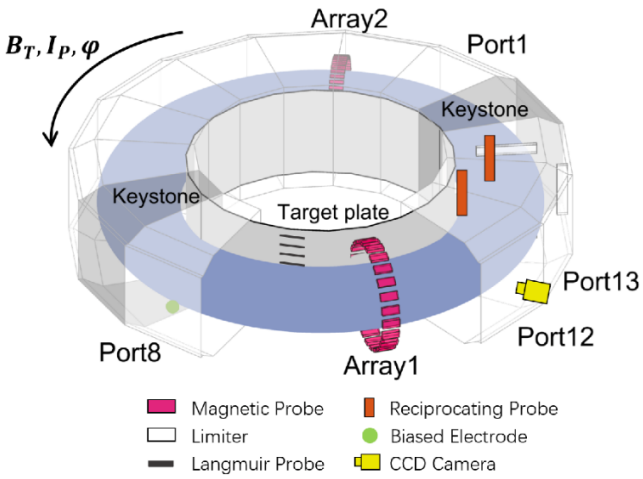

Figure 1. Schematic diagram of the J-TEXT tokamak device. Spatial distribution of diagnostic equipment, limiter and biased electrode

Since the J-TEXT tokamak is equipped with divertor coils, it can operate in the poloidal divertor configuration. Significantly different from general tokamak devices, the divertor coils of J-TEXT are installed on the high field side, so the X-point formed by the divertor coils and plasma is on the high field side. Depending on the number of X points and different locations, the divertor

configuration of J-TEXT can be divided into four types: upper single null (USN), lower single null (LSN), double null (DN) and mid-plane single null (MSN). In this paper, the SOL biasing experiments are implemented in the MSN configuration. The spatial distribution of plasma separatrix, biased electrode, reciprocating probes and DLP in MSN configuration is shown in figure 2. Due to the limitation of the number of signal acquisition channels, only the probe near the strike points is used. The arrows marked white are the probes that normally work in the experiment, and the black arrows are the probes that do not work. Figure 2 shows that the low-field side limiter is relatively close to the plasma separatrix. In the experiment, due to the unstable control of plasma horizontal displacement, the plasma separatrix is easy to contact the low-field side limiter and change into the limiter configuration or the limiter will partially enter SOL, which is very unfavorable for the SOL biasing experiment. Figure 3 shows the basic parameters such as plasma horizontal displacement d_X and SOL current I_{SOL} generated by the electrode in the regular discharge.

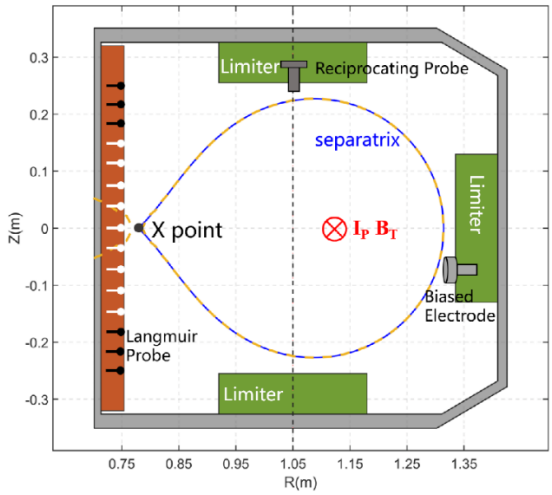

Figure 2. Spatial position of plasma separatrix, divertor target plate probes, reciprocating probes and electrode in the MSN configuration.

The change of SOL current is closely related to the horizontal displacement. When the horizontal displacement is positive, the plasma moves to the low field side, leading to the electrode moving deeper into SOL. The increase of plasma parameters at the electrode leads to a larger SOL current. In the experiment, the current generated by the biased electrode will flow along the SOL open magnetic field line to the divertor target plate. Because the target plate is connected to two vacuum chambers, the current I_V collected by one vacuum chamber is almost half of the SOL current.

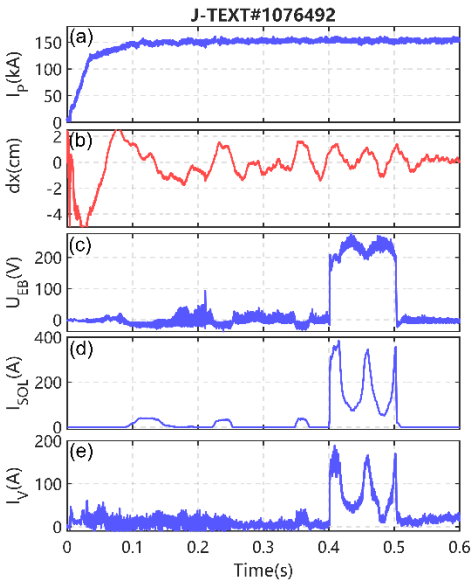

Figure 3. Basic parameters of the SOL biasing experiment. (a) plasma current, (b) horizontal displacement of the plasma, (c) voltage applied to the electrodes, (d) SOL current driven by the electrode, (e) current collected by one vacuum chamber.

The data presented in this paper are the results of two rounds of experiments in autumn 2020 and spring 2021. The physical view of the electrode is shown in figure 4. The diameter of the electrode in the first round is 4 cm, while in the second round it's 5 cm. Under the same conditions, the larger the electrode size is, the larger the SOL current will be.

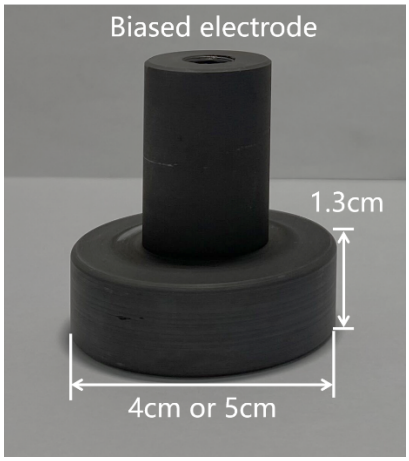

Figure 4. Physical picture of biased electrode.

3. Effects of SOL current on plasma

In SOL biasing experiment, it is observed that the electron density, ion saturation current, floating potential, plasma velocity and radial electric field measured by Langmuir probe have significant changes during the process of applying voltage to the electrode. CCD camera captured the phenomenon similar to the strike points splitting caused by RMPs. The poloidal magnetic fields

generated by SOL current are also measured by two sets of poloidal magnetic probe arrays. These experimental results will be divided into three parts to describe. Section 3.1 briefly describes the basic characteristics of SOL current in the MSN configuration and the simulation results by SOL current model. Secondly, section 3.2 describes the influence of SOL current on SOL plasma parameters. Finally, section 3.3 describes the influence of SOL current on the upper and lower strike points, the change of visible light radiation at the strike points photographed by CCD camera and simulations showing lobes excited by magnetic perturbations generated by SOL current near the X-point.

3.1 Basic characteristics of SOL current in the MSN configuration

In the previous work, the SOL current driven by the biased electrode in the limiter configuration has been confirmed on J-TEXT [40], so the biased electrode can still drive SOL current in the divertor configuration. The experimental results of discharge #1072089 are presented here, in which the biased electrode is applied with 300V square wave voltage of 1kH and duty ratio of 0.5. Figure 5(a) and (b) shows the poloidal magnetic field generated by the SOL current measured by the poloidal magnetic probe arrays 1 and 2. Figure 5(c) shows the SOL current driven by the biased electrode.

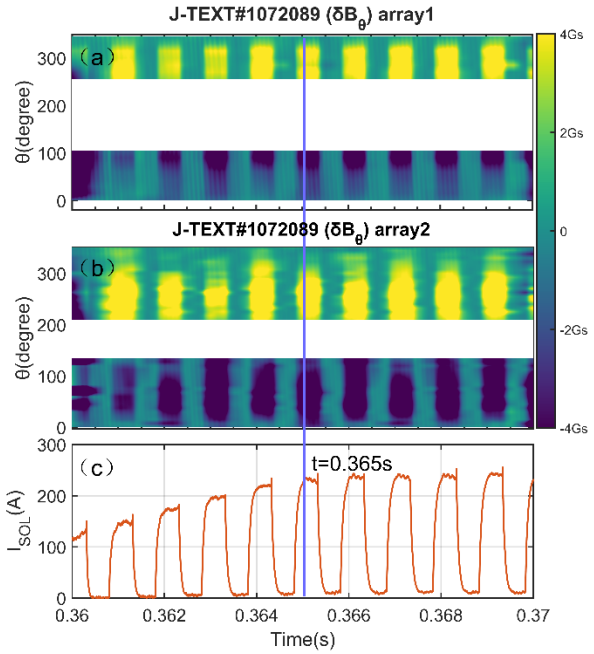

Figure 5. Variation of poloidal magnetic field with SOL current measured by magnetic probe array. (a) array1, (b) array2, (c) SOL current. The blank part is the missing magnetic probe data. The blue solid line indicates that the model has chosen the 0.365 s moment for the simulation.

Magnetic probes at the high field side of arrays 1 and 2 are removed to meet the requirements of the discharge in the divertor configuration. The blank part in figure 5(a) and (b) is the missing magnetic probe data in the high field side. Results shows that the larger the SOL current is, the larger the amplitude of the perturbation magnetic field will be. Discharge #1072089 is simulated by using the SOL current model previously developed [41]. As shown in figure 6(a), the SOL current driven by the electrode is divided into two parts. The orange current is in the same direction as the plasma current, and the blue current is in the opposite direction as the plasma current. The forward current flows to the lower target plate, the reverse current flows to the upper target plate, and the SOL current is basically distributed equally to the two vacuum chambers. Therefore, the entire SOL current path is simpler than that in the limiter configuration [41]. The amplitude of the poloidal magnetic field generated by the orange SOL current is positive, while the amplitude of the poloidal magnetic field generated by the blue SOL current is negative. The poloidal angles of the middle

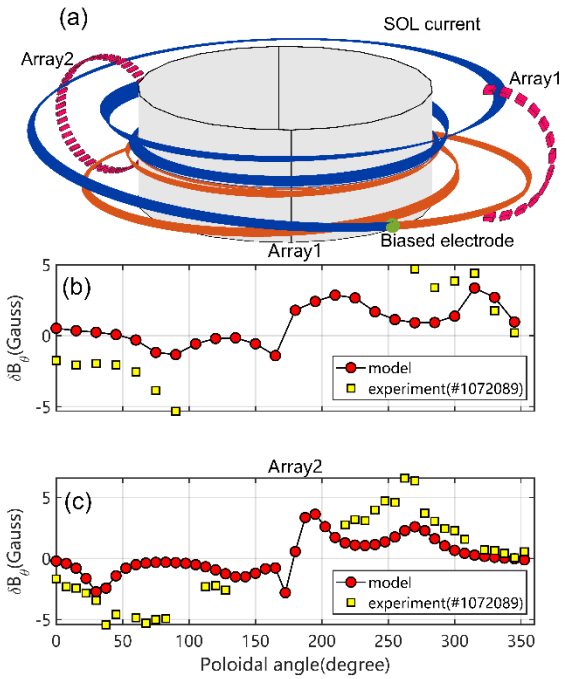

Figure 6. (a) The SOL current path calculated by the model, with the orange current following the direction of the plasma current and the blue current in the opposite direction. (b) and (c) are the magnetic fields measured by the two magnetic probe arrays and the simulated magnetic fields, respectively.

plane of the low field side and the middle plane of the high field side are defined as $\theta = 0°$ and $\theta = 180°$ respectively, and the θ direction is counterclockwise. Since the orange SOL current is below

the middle plane ($180° < \theta < 360°$) while the blue SOL current is above the middle plane ($0° < \theta < 180°$), so the magnetic field generated by the SOL current measured by the magnetic probe and calculated by the model are both positive below the middle plane and negative above. Although the data of the magnetic probe in the high field side are missing, the simulation results are basically consistent with the experimental measurements. Combined with figure 6(a) and (c), it can be seen that the closer the SOL helical current filaments is to the magnetic probe, the greater the poloidal magnetic field will be generated. The simulation results are basically smaller than the experimental measured values, which may be because the magnetic field generated by SOL current changes the magnetic topology of boundary plasma and then changes the original path of SOL current, and a more detailed discussion is presented in section 4.1. As shown in figure 7, SOL current produces strong boundary resonance components on the last closed flux surface (LCFS) or separatrix, which implies that the SOL current has the potential to control ELMs when it is large enough. The safety factor in the SOL region where the electrode is located is similar to that of the pedestal region, and the SOL current is closer to the boundary plasma leading to generating more efficient RMPs.

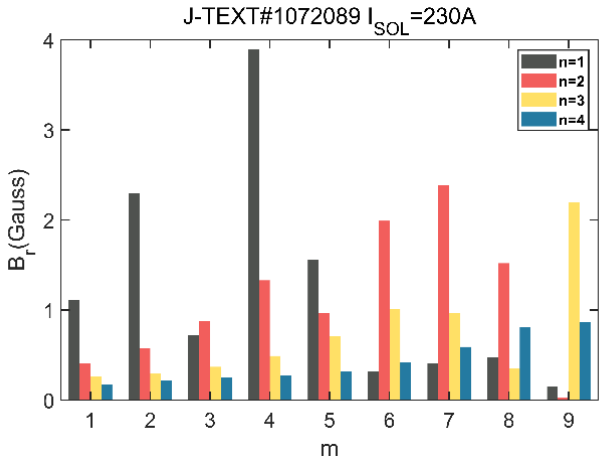

Figure 7. Radial magnetic field components obtained by the model at the LCFS generated by the SOL current. SOL current driven by the biased electrode can produce strong boundary resonance components such as 4/1, 7/2, 9/3, etc.

3.2 The impact of the SOL current on the plasma parameters

Two sets of reciprocating probes installed in port12 and port13 are used to measure the boundary plasma parameters. The parameters such as floating potential and ion saturation current measured by the probe change significantly during the process of applying bias voltage to the electrode. The

rake probe at port12 consists of six single probes in different radial positions with a radial distance of 5 mm between each probe. In the discharge #1072090, the electrode is located in SOL and 300V square wave voltage of 1kH is applied. Figure 8 shows the variation of the floating potential with SOL current at six radial positions measured by the rake probe. The radial position of the electrode with respect to the center of the vacuum chamber is fixed during the application of bias. The relative distance between the electrode and the plasma separatrix is constantly changing due to the instability of the plasma horizontal displacement. The plasma displacement reflects the movement of the center of gravity of the plasma current. Therefore, r_{EB} is defined here as the actual relative distance between the electrode and the plasma current center of gravity after considering the horizontal displacement. As shown in figure 8, the smaller the r_{EB} is , the higher the plasma parameter at the electrode and the larger the SOL current I_{SOL}. From the comparison of Fig. 8 (a) (b) and (c) it can be seen that the variation of the floating potential is proportional to the amplitude of the SOL current, which also indicates that the penetration depth of the potential perpendicular to the magnetic field lines caused

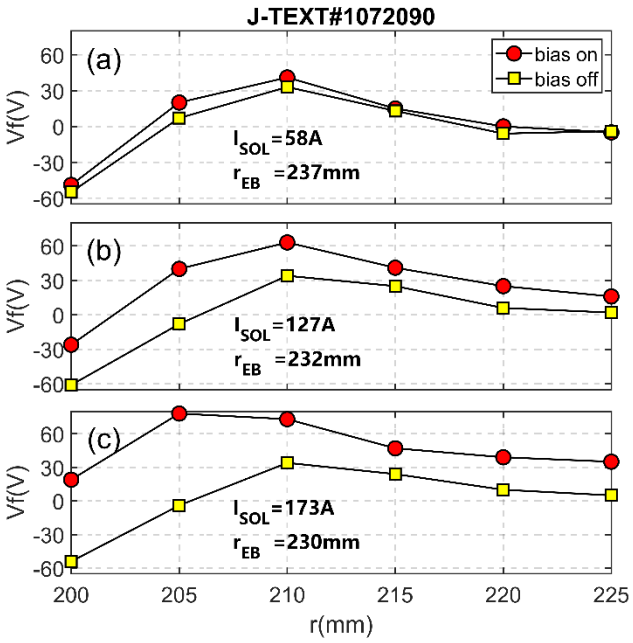

Figure 8. The effect of different SOL current amplitudes on the plasma floating potential, red markers indicate that the electrode is biased, yellow markers indicate that the electrode is not biased. (a) SOL current is 58 A, (b) SOL current is 127A, (c) SOL current is 173 A.

by the SOL current is at least a few centimeters. After the bias voltage is applied to the electrode, a smaller current has no significant change on the floating potential, and the amount of change in

potential increases as the current gradually increases. As the radial position of the plasma decreases, the change in the floating potential here becomes more significant. The increase in floating potential does not exceed thirty percent of the bias voltage amplitude applied to the electrode. The floating potential measured at the radial position r = 200 mm is negative without bias applied to the electrode, which proves that the single probe is inside the magnetic separatrix, and the SOL current has an effect not only on the SOL plasma but also on the confined plasma within the separatrix. Since the limited J-TEXT diagnostic equipment can only provide one-dimensional distribution of the plasma floating potential in the radial direction at one toroidal position, it is crucial to obtain three-dimensional distribution of the plasma potential since the SOL current itself is distributed in space in three dimensions.

In the discharge #1072092, the electrode is also located in SOL and 300V square wave voltage of 1kH is applied. Due to the unstable horizontal displacement control in the MSN configuration, the period from 0.382 s to 0.387 s when the horizontal displacement is stable is selected to reduce the measurement interference caused by the horizontal displacement. Therefore, figure 9 shows the variation of plasma parameters measured by reciprocating probe with SOL current during this period. The reciprocating probe is located at SOL, and figure 9(a), (b), (c), (d), (g) and (h) are floating potential, ion saturation current, electron temperature, and electron density, SOL current, biased electrode position respectively. Figure 9(e) and (f) respectively show the plasma toroidal velocity and radial electric field changed after the input of bias. All SOL plasma parameters are increased when positive bias is applied. The increase in electron temperature and density perturbation is about ten percent of the equilibrium parameter. In particular, the plasma toroidal velocity increases by 10 km/s when the bias is applied. In figure 9(e), the black line is the plasma toroidal velocity measured by Mach probe, while the blue line is the drift velocity of $E_r \times B_\theta$ calculated by the measured ΔE_r divided by B_θ. The trend of the two lines is almost identical, suggesting that the increase of plasma toroidal velocity is indeed caused by $E \times B$ drift. The increase in plasma parameters may be due to several reasons:

(a) The ohmic heating power on the J-TEXT tokamak is approximately 300 kW. The power input to the plasma from the biased electrode is 45 kW, which corresponds to the auxiliary heating of the SOL plasma. As for the absorption efficiency of the power injected into SOL by the electrode is not clear.

(b) Experiments on EAST using LHW and TORPEX using biased electrodes have controlled the blob [25,47], and experimental results on EAST suggest that $E_r \times B$ flow shear plays an important role. Experiments on J-TEXT show that SOL current does enhance the radial electric field, so SOL current may suppress the SOL turbulence or blob behavior resulting in reduced radial transport losses. The study of blob behavior is beyond the scope of this manuscript, it can be the work later.

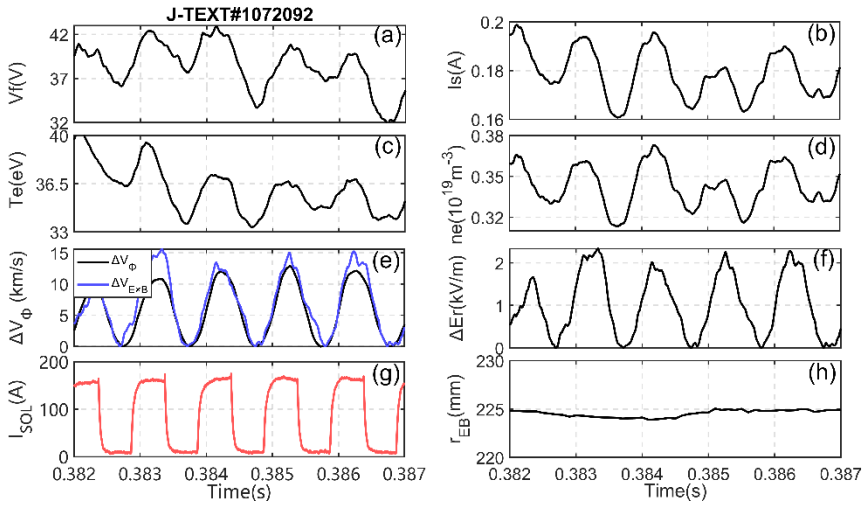

Figure 9. Variation of plasma parameters with SOL current measured by reciprocating probe, (a) plasma floating potential, (b) ion saturation current, (c) electron temperature, (d) electron density, (e) comparison of toroidal flow velocity measured by Mach probe and toroidal drift velocity calculated using ΔE_r, (f) variation of radial electric field, (g) SOL current driven by electrode, (h) distance between electrode and center of gravity of plasma current.

3.3 The impact of the SOL current on the boundary magnetic topology

One of the visible light radiation diagnostics on J-TEXT is the CCD camera, which has a frame rate of 500 frames per second and typically operates for 2s. In SOL biasing experiment, plasma radiation changes near electrode and target plate are mainly taken. Since CCD camera works normally in the second experiments, the results of the second experiments are described here. In discharge #1076492, in which the biased electrode is applied with 350V DC. Figure 10 shows the changes of strike points taken by CCD camera at different times. The white arrows in the figure refer to the secondary strike points, and the blue arrows refer to the primary strike points. The amplitude of SOL current is different at different time due to the different distance between plasma separatrix and electrode. When the SOL current is large, the temperature at the electrode is higher, resulting in more carbon impurities being sputtered from the electrode and stronger visible

light radiation. When the SOL current driven by the electrode reaches 110A, the strike points splits obviously at the upper target plate, while there is no significant variations at the lower strike points. As the SOL current increases, the magnetic perturbation generated by the SOL current is also greater, resulting in more significant strike points splitting. At 0.505s, the strike points splitting disappears without bias. Due

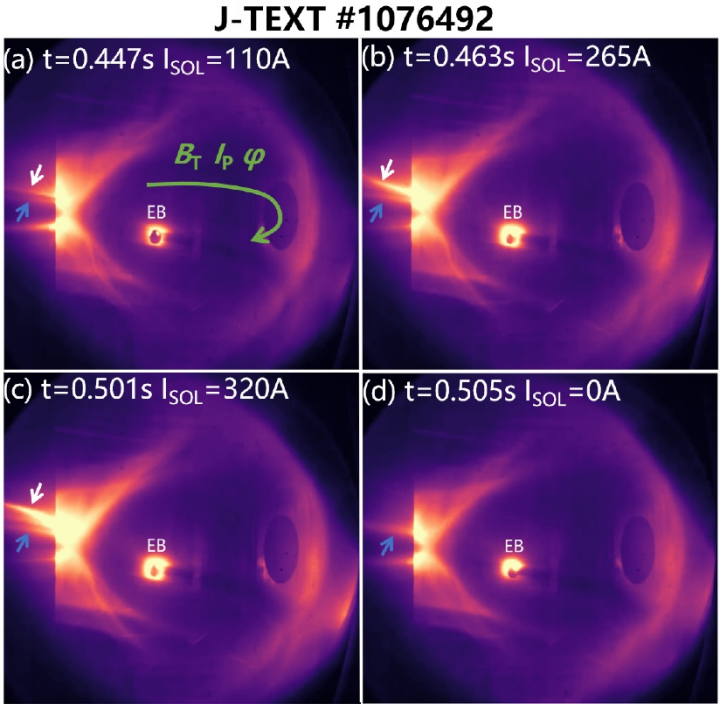

Figure 10. Variation of visible light radiation throughout the plasma at different moments with different SOL current amplitudes. Figures (a) (b) and (c) show clear strike points splitting at the upper target plate with bias, while figure (d) shows no strike points splitting without bias. The blue arrow indicates the primary strike points, the white arrow indicates the secondary strike points, and the green arrow points to the plasma current direction.

to the low spatial resolution of the DLP, the distance between each probe is 3.8 cm. Measurements of the DLP show no clear strike points splitting. In order to understand the appearance of the strike points splitting, the perturbation magnetic field generated by the SOL current is calculated in the SOL current model using the vacuum assumption and then superimposed with the equilibrium magnetic field calculated by EFIT, and the Poincaré diagram of the plasma boundary is obtained by magnetic field line tracing. The 0.463s moment of discharge #1076492 is used for the simulation with the SOL current of 265A. As shown in figure 11(a), it is found that the presence of lobes structure above the X-point implied that the upper strike points splitting is caused by it. In figure 11(b), the length of lobes changes becomes shorter in another toroidal position, which

implies that the lobes is three-dimensional asymmetric structures. By tripling the SOL current to 795 A, the lobes becomes longer and directly connected to the target plate as in figure 11(c). Figure 11(d) also shows the lobes becoming larger in another toroidal position compared to figure 11(b). Lobes create some additional channels for the main plasma to connect to the divertor target plate, allowing particles from the core to be transported to the target plate causing the strike points splitting. This is the first time that strike points splitting has occurred using SOL currents instead of RMPs coils in the divertor configuration on the J-TEXT tokamak.

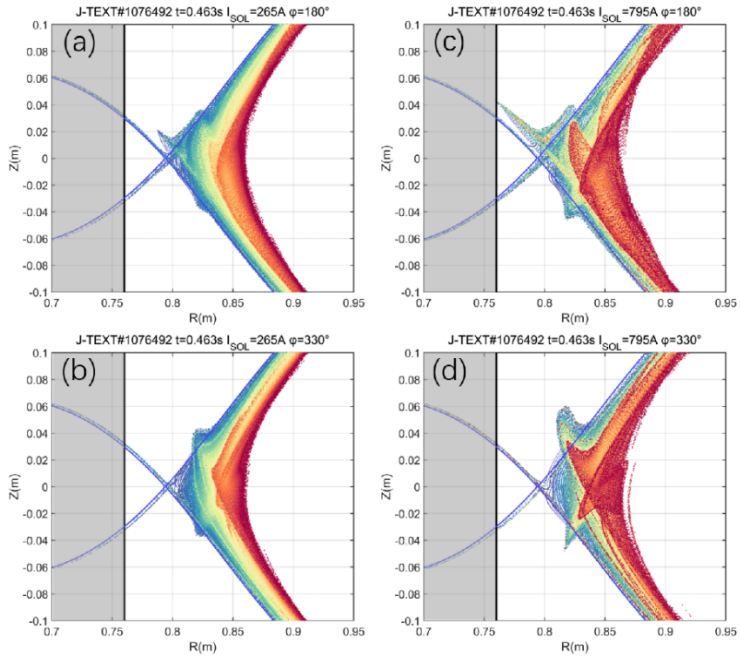

Figure 11. Poincaré diagrams for different SOL current amplitudes at different toroidal positions. (a) I_{SOL} = 265 A, φ = 180°, (b) I_{SOL} = 265 A, φ = 330°, (c) I_{SOL} = 795 A, φ = 180°, (d) I_{SOL} = 795 A, φ = 330°. Simulation results show that lobes appear near X-point.

4 Discussion

For the above experimental phenomena, the physical mechanisms behind them may be complex, and some possible explanations for them are presented in this discussion. First, section 4.1 describes the possible reasons why the magnetic field generated by the SOL current measured by the magnetic probe differs from the simulation results. Secondly, section 4.2 briefly describes how SOL currents cause changes in the plasma potential. Finally, Section 4.3 describes the effect of plasma horizontal displacement on the SOL current amplitude and its induced the difference of upper strike points splitting.

4.1 The difference between the simulated and experimental magnetic field generated by the SOL current

In section 3.1, the B_θ generated by the SOL current calculated by the model is smaller than that generally measured by the magnetic probe. There may be three reasons for this error. The first reason is that the perturbation magnetic field generated by SOL current itself will change the equilibrium magnetic field, thus changing the path of SOL current. Of course, this may require the superposition of the equilibrium magnetic field and the perturbation magnetic field of the initial calculation, and then tracking the path of the SOL current for the second perturbation magnetic field calculation. The above process is repeated until the path of SOL current remains unchanged, which means the convergence of iteration. The second reason is that the existence of cross-field current is not considered, only the magnetic field generated by SOL current parallel to the magnetic field line is considered, and the path of cross-field current and its corresponding magnetic field cannot be calculated by this model. The third reason is that, similar to the response of a plasma to the amplification or shielding effect of applied RMPs, the plasma actually responds to the perturbation magnetic field generated by the SOL current. Here the plasma appears to amplify the magnetic field generated by the SOL current. However, the response of plasma to SOL current is beyond the scope of this paper. In the future, the single-fluid resistive MHD code similar to MARS-F [48] or M3D-C1 [49] can be used to study the response of plasma to SOL current.

4.2 Potential penetration caused by SOL current

According to the theory of plasma sheath, the plasma sheath will be formed on the electrode surface if the electrode is not biased, and the electrons and ions in the sheath will form bipolar transport to maintain electric neutrality. Under the positive bias, the SOL current driven by the biased electrode will form electron sheaths and ion sheaths on the electrode surface and target plate surface respectively. Due to the generation of net current in the sheath, the condition of bipolar transport is no longer met, but the whole SOL current circuit meets macro bipolar transport, which means that the total electron flux lost by all conductors is equal to the total ion flux. Only when the ratio of the biased conductor area to the unbiased conductor area is less than a certain value can the electron sheath be formed and the electron saturation current be driven [50].

In J-TEXT tokamak, the ratio of electrode surface area to target surface area is very small.

The maximum current driven by the biased electrode is electron saturation current, which implies that the current density on the electrode surface is much larger than that on the target plate surface, so the SOL current is not strictly parallel to the magnetic field line and needs to cross the magnetic field line to connect to a larger range of grounded target plate. Here, the flux tube connected to the electrode is defined as biased flux tube (BFT). In figure 12, L is the flux tube length connecting electrode and target plate, the blue line is the change of plasma potential without bias with L, and

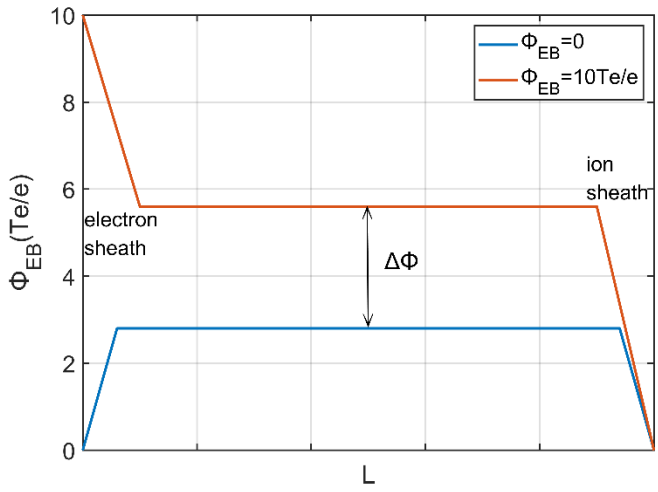

Figure 12. The flux tube connects the electrode to the target plate and the plasma potential varies with the connection length L of the flux tube. The electron and ion sheaths are formed at both ends of the biased flux tube, and the ion sheaths are formed at both ends of the unbiased flux tube. Due to the Debye shielding effect of the sheath, the voltage drop is concentrated in the plasma sheath at both ends of the flux tube.

the red line is the change of plasma potential with positive bias. After positive bias is applied, the potential drops sharply in the sheath layer at both ends of the flux tube. The potential platform region in the BFT is SOL plasma potential, and $\Delta\Phi$ is the increase of plasma potential. The potential difference between the biased flux tube and the unbiased flux tube will generate electric field to drive the cross-field current, which will also cause $E\times B$ drift, resulting in the generation of convective cells [22,25,51]. Convective cells will increase the thermal decay length λ_q of SOL and reduce the thermal load of the target plate [23], which is beyond the scope of this paper. As shown in the figure 8, when the SOL current driven by the electrode is larger, the cross-field current loss perpendicular to the field line becomes larger, which may increases the plasma potential in the biased flux tube in order to drive stronger cross-field current, resulting in the increase of floating potential. Due to the strong magnetic shear near X-point, the size of the BFT connected to the

electrode will be squeezed to less than the ion cyclotron radius [51]. At the same time, the potential perturbations generated by the electrode should not cross the separatrix and affect the confined plasma. However, figure 8 shows that the negative floating potential at r = 200 mm without bias implies that the potential change caused by the SOL current has crossed the separatrix, the penetration of the potential is similar to the penetration of the magnetic surface caused by lobes.

4.3 The relationship between strike points splitting and plasma horizontal displacement

Due to the unstable control of plasma horizontal displacement in the divertor configuration, the shape and position of plasma constantly change, which also makes the SOL current driven by the electrode and the magnetic perturbations generated by it change. Figure 13 shows the equilibrium reconstruction calculated by EFIT at different times in discharge #1076492. The size and spatial

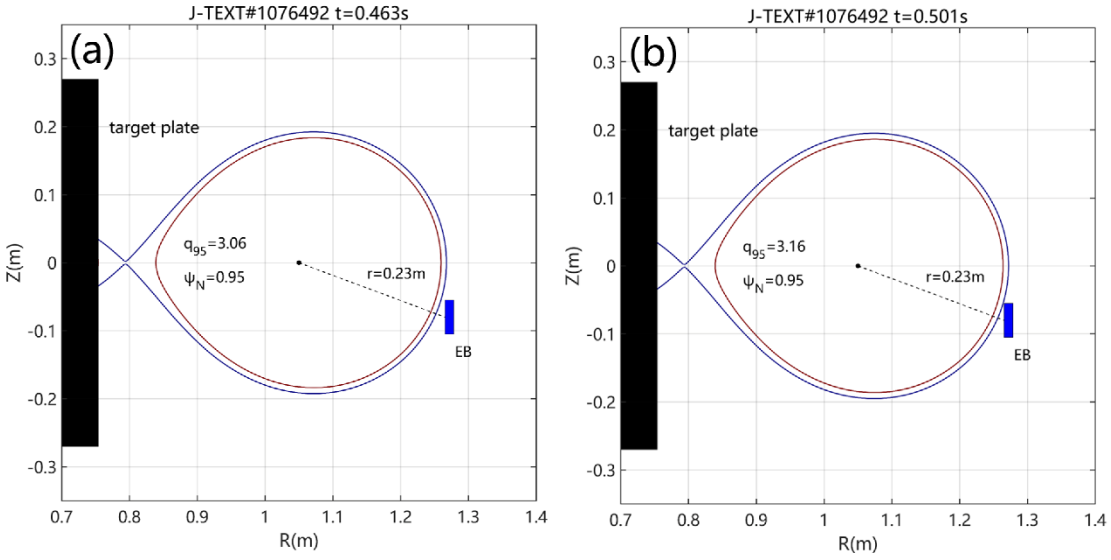

Figure 13. The equilibrium reconstruction of the plasma at different moments, q_{95} and the distance from the electrode to the LCFS are significantly changed. (a) t = 0.463 s, (b) t = 0.501 s.

position of the electrode in the schematic diagram are the actual values in the experiment. The radial position of the electrode center relative to the vacuum chamber center is 0.23 m, and the major radius of the divertor target plate is 0.754 m. At 0.501s, the electrode is closer to the magnetic separatrix so that the SOL current is larger, and the value of q_{95} is also larger than that of 0.463 s. As shown in figure 10, the larger the SOL current is, the more obvious the strike points splitting will be. The simulation of strike points splitting on JET shows that the change of q_{95} and

error field correction coils (EFCC) current has a significant impact on the lobes, leading to the difference of strike points splitting on the target plate[16]. The plasma horizontal displacement on J-TEXT not only changes q_{95} but also changes the SOL current amplitude, which may also lead to different plasma responses to SOL current and strike points splitting. Since the structure of the SOL current itself is also included, the physical mechanism contained in the photographs taken by the CCD camera is more complex. In the future, the divertor Langmuir probe will be upgraded to provide higher poloidal spatial resolution for the measurement of strike points splitting, and an infrared camera will be installed to measure the thermal load of the target plate. The control of plasma horizontal displacement in the divertor configuration is also being improved.

5 Conclusion

The SOL current has complex effects on the plasma, such as changing the magnetic topology of the boundary plasma, changing the potential of the SOL plasma causing $E \times B$ drift and thus affecting the thermal load distribution of the target plate, the interaction of the SOL current with the MHD instabilities, etc. Due to the limited auxiliary heating power, the J-TEXT tokamak is currently not capable of H-mode operation and therefore the control effect of SOL currents on ELMs cannot be studied. The experimental results show that the amplitude of the SOL current is closely related to the plasma parameters at the electrode, and also the SOL current changes the plasma parameters. Since the electrode in the SOL generates a large amount of impurities, it is desirable to utilize biased target plates to drive the SOL current in future fusion devices. The experiments on J-TEXT provide major references for other devices to carry out experiments on active control of ELMs using SOL currents. In future work, the response of the plasma to the SOL current, the change in the heat load distribution of the target plate caused by the SOL current are important. Simulation work can be carried out using fluid codes such as EMC3-EIRENE, SOLPS, etc. SOL biasing experiments in double-null configuration and applied ECRH auxiliary heating will also be the next step.

Acknowledgements

This work is supported by the National Key R&D Program of China (No. 2017YFE0301100), the

National Natural Science Foundation of China (Contract No. 11905078, 12075096, 12047526, and No. 51821005) and “the Fundamental Research Funds for the Central Universities” under Grant No. 2020kfyXJJS003.

Reference

[1] Loarte A. *et al* 2003 *Plasma Phys. Control. Fusion* 45 1594
[2] Y. Liang. *et al* 2007 *Phys. Rev. Lett.* 98 265004
[3] Y. Liang. *et al* 2010 *Nucl. Fusion* 50 025013
[4] W. Suttrop. *et al* 2011 *Phys. Rev. Lett.* 106 225004
[5] Y. Sun. *et al* 2017 *Nucl. Fusion* 57 036007
[6] Liang Y. *et al* 2013 *Phys. Rev. Lett.* 110 235002
[7] Jeon Y.M. *et al* 2012 *Phys. Rev. Lett.* 109 035004
[8] T. Evans. *et al* 2004 *Phys. Rev. Lett.* 92 235003
[9] T. Evans. *et al* 2008 *Nucl. Fusion* 48 024002
[10] T. Evans. *et al* 2006 *Nat. Phys.* 2 419–23
[11] Kirk A. *et al* 2010 *Nucl. Fusion* 50 034008
[12] Kirk A. *et al* 2012 *Phys. Rev. Lett*. 108 255003
[13] J.R. Harrison. *et al* 2014 *Nucl. Fusion* 54 064015
[14] J.-W. Ahn. *et al* 2010 *Nucl. Fusion* 50 045010
[15] M.W. Shafer. *et al* 2012 *Nucl. Fusion* 52 122001
[16] D.M. Harting. *et al* 2012 *Nucl. Fusion* 52 054009
[17] R. A. Moyer. *et al* 2018 *Rev. Sci. Instrum.* 89 10E106
[18] T. Evans. *et al* 2005 *J. Phys.: Conf. Ser*. 7 174
[19] S. Xu. *et al* 2018 *Nucl. Fusion* 58 106008
[20] M. Rack. *et al* 2014 *Nucl. Fusion* 54 064016
[21] S J Zweben. *et al* 2009 *Plasma Phys. Control. Fusion* 51 105012
[22] S J Zweben. *et al* 2012 *Plasma Phys. Control. Fusion* 54 105012
[23] Hara J. *et al* 1997 *J. Nucl. Mater.* 241 338
[24] T. Shoji. *et al* 1995 *J. Nucl. Mater.* 220 357
[25] C. Theiler. *et al* 2012 *Phys. Plasmas* 19 082304
[26] C. Theiler. *et al* 2012 *Phys. Rev. Lett.* 108 065005
[27] G.F. Counsell. *et al* 2003 *J. Nucl. Mater.* 313 804
[28] C.G. Silva. *et al* 1999 *J. Nucl. Mater.* 266 679
[29] S.J. Fielding. *et al* 2001 *J. Nucl. Mater.* 290 859
[30] M.J. Schaffer. *et al* 1992 *Nucl. Fusion* 32 855
[31] John W. Brooks. *et al* 2021 *Nucl. Fusion* 61 096017
[32] J.P. Levesque. *et al* 2017 *Nucl. Fusion* 57 086035
[33] B.T. Cui. *et al* 2021 *Fusion Eng. Des.* 173 112963
[34] Liang Y. *et al* 2019 *Nucl. Fusion* 59 112016
[35] Ding Y H. *et al* 2018 *Plasma Sci. Technol.* 20 125101
[36] Zhu T. *et al* 2014 *Rev. Sci. Instrum.* 85 053504
[37] Chen Z. *et al* 2021 *Nucl. Fusion* 61 026001

[38] Liu H. *et al* 2017 *Nucl. Fusion* 57 016003
[39] Sun Y. *et al* 2014 *Plasma Phys. Control. Fusion* 56 015001
[40] Wang N. *et al* 2019 *Nucl. Fusion* 59 096047
[41] Li S. *et al* 2021 *Plasma Phys. Control. Fusion* 63 115017
[42] Han D. *et al* 2021 *Plasma Sci. Technol.* 23 055104
[43] Joseph I. 2009 *Phys. Plasmas* 16 052510
[44] Joseph I. 2009 *Phys. Plasmas* 16 052511
[45] Joseph I. 2012 *Phys. Plasmas* 19 056124
[46] Wang H. *et al* 2021 *Plasma Sci. Technol.* 23 125103
[47] Wang Q. *et al* 2019 *Phys. Plasmas* 26 072305
[48] Liu Y. *et al* 2005 *Nucl. Fusion* 45 1131
[49] S. Munaretto. *et al* 2022 *Nucl. Fusion* 62 026018
[50] Zhang H, Li D and Liang Y. 2020 *Plasma Sci. Technol.* 10 105102
[51] D D Ryutov. *et al* 2001 *Plasma Phys. Control. Fusion* 43 1399–1423